INSTITUTE OF PHYSICS PUBLISHING WAVES IN RANDOM MEDIA

Waves Random Media **12** (2002) 47–62 PII: S0959-7174(02)22650-6

# Electromagnetic propagation in a curved two-dimensional waveguide

**M Spivack**[1], **J Ogilvy**[2] **and C Sillence**[2]

[1] Department of Applied Mathematics and Theoretical Physics, The University of Cambridge, Cambridge CB3 9EW, UK
[2] BAE SYSTEMS, Advanced Technology Centre—Sowerby, Filton, Bristol BS34 7QW, UK

E-mail: ms100@cam.ac.uk

Received 8 March 2001, in final form 2 October 2001
Published 30 October 2001
Online at stacks.iop.org/WRM/12/47

**Abstract**

Fields due to an electromagnetic wave propagating in a long irregular two-dimensional waveguide are calculated efficiently, using the method of left–right splitting to solve the coupled integral equations. Results are compared with those obtained from independent ray-theoretic calculations and give very close agreement. The approach has previously been applied to rough surfaces at low angles of incidence; here it is found to converge rapidly for surface slopes of 30°, and after a few iterations for incident angles up to 60° from grazing.

## 1. Introduction

In many important electromagnetic and acoustic applications the wavefield propagates along an irregular or curved waveguide and becomes progressively scattered (e.g. [1–5]). This is the case in problems such as optical fibres and acoustic propagation in shallow water [6, 7]. Although exact solutions for some canonical geometries are among the earliest work in this area [8, 9], numerical treatment is necessary for more general cases, for which computational problems remain acute and diffraction phenomena are often inadequately understood. This is particularly so for elongated, narrow or randomly rough waveguides where diffraction effects dominate.

Treatment is possible in principle by a full solution of the boundary integrals arising from Maxwell's equations, but even in two dimensions this quickly becomes prohibitively expensive for large waveguides. Even where radii of curvature are large, and approximate solutions such as ray theory are locally valid, the number of rays needed rises steeply with the waveguide length to avoid loss of coherence. On the other hand, in many cases wave propagation is predominantly forward going, at least locally, and this suggests the use of 'left–right splitting' recently proposed to simplify the full boundary integral problem.

  

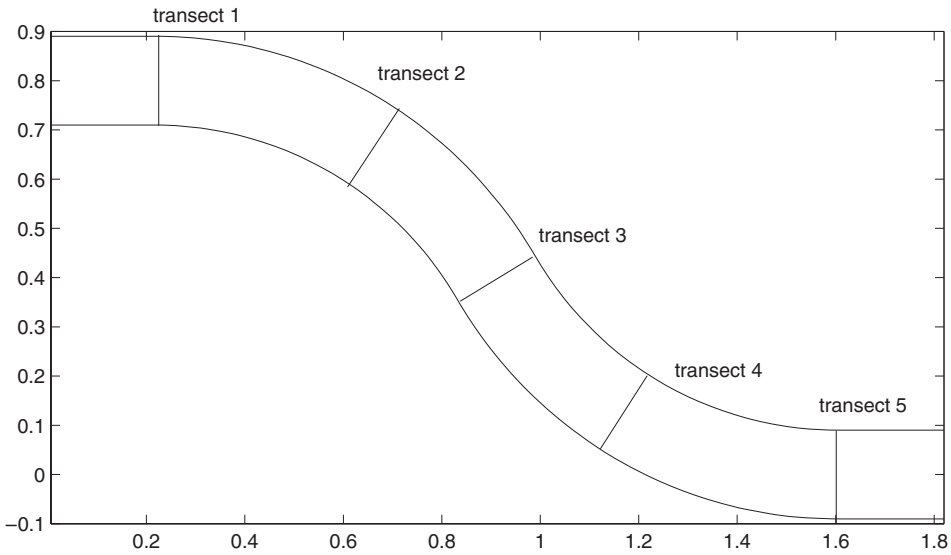


**Figure 1.** Geometry of the waveguide, showing the five transects at which detailed comparison of fields is made.

The aims of this paper are twofold. The first is to develop an accurate numerical solution for long irregular waveguides. The second is to validate the solution by careful comparison of the interior fields with independent calculations at various distances along the waveguide. In addition the convergence of the solution is examined for large angles of incidence with respect to grazing, where high multiple scattering arises.

The method is adapted from that of left–right splitting, applied previously to rough surfaces at low grazing angles (e.g. [10–12]). The full Helmholtz equations give rise here to a pair of coupled integral equations along the two surfaces. The solution to this system is expressed as a series in increasingly high orders of multiple scattering, in which the first term gives purely forward scatter. (The approach takes fully into account the interaction between the surfaces, which becomes increasingly important for narrow waveguides.) For illustration we concentrate on a waveguide of 20 wavelengths in width and 200 in length. Surface slopes in this case vary between $0^\circ$ and around $45^\circ$. Surface currents for this are obtained rapidly, giving extremely close agreement with independent calculations when used to obtain interior fields. For angles up to around $20^\circ$ the first one or two terms are very accurate. Although designed to deal with low grazing angles, the approach also converged in about five iterations for angles of incidence as large as $60^\circ$ from grazing.

The paper is organized as follows: in section 2 the coupled boundary integral equations are formulated, and the formal series solution is described. The numerical treatment is briefly described in section 3. In section 4 the main results are given, examining the accuracy and convergence in several cases and illustrating the effect of roughness.

## 2. Formulation of equations

We shall consider the fields due to electromagnetic propagation along a curved waveguide. The underlying geometry is shown in figure 1. Five one-dimensional transects are chosen, at which fields are calculated by the two methods for a detailed comparison. These are also

shown in figure 1. The upper and lower surfaces are perfectly conducting and denoted $S_1$ and $S_2$ respectively. Typically the waveguide will have a depth of around 20 wavelengths and a length of around 200 wavelengths. The field in the waveguide can be written as a boundary integral over the normal derivative along the surfaces. The left-hand end will be treated as an aperture, $A$. The electric field incident on this aperture may be taken to be a horizontally or vertically polarized plane wave, i.e. corresponding to TE or TM. We will assume here a TM field, and consider the magnetic field $H$, so that $H$ obeys the Helmholtz wave equation $(\nabla^2 + k^2)H = 0$. Let $G$ be the free space Green function, so that $G$ is the zero-order Hankel function of the first kind,

$$G(\boldsymbol{r}, \boldsymbol{r}') = \frac{1}{4\mathrm{i}} H_0^{(1)}(k|\boldsymbol{r} - \boldsymbol{r}'|). \tag{1}$$

Here $\boldsymbol{r} = (x, z)$ where $x$ and $z$ denote horizontal and vertical coordinates respectively.

The initial goal is to find the surface currents along the waveguide, and then use these to obtain the interior fields. The field at a point $\boldsymbol{r}$ inside the waveguide can be expressed as an integral across the bounding surfaces:

$$H_s(\boldsymbol{r}) = H_{\mathrm{inc}}(\boldsymbol{r}) + \int_S \left[ \frac{\partial G(\boldsymbol{r}, \boldsymbol{r}')}{\partial \boldsymbol{n}} H(\boldsymbol{r}') \right] \mathrm{d}r' \tag{2}$$

where $\boldsymbol{n}$ denotes the normal outward from the waveguide, $\boldsymbol{r}_s = (x, S(x))$, $\boldsymbol{r}' = (x', S(x'))$ and $S$ is the union of the two surfaces. Taking limits as $\boldsymbol{r}$ tends respectively to the upper and to the lower surfaces, and applying the boundary conditions, we obtain two coupled integral equations for the unknown values of the quantity $H$ along each of the two surfaces. It is convenient to regard these as separate functions of the single coordinate $x$, and accordingly we define

$$\begin{aligned} \Psi_1(x) &= H(x, S_1(x)) \\ \Psi_2(x) &= H(x, S_2(x)). \end{aligned} \tag{3}$$

The coupled integral equations for $\Psi_1$, $\Psi_2$ can then be written

$$\begin{aligned} H_{\mathrm{inc}}(\boldsymbol{r}_1) &= \int_S \left[ G_n(\boldsymbol{r}_1; \boldsymbol{r}_2')\Psi_2(x') - G_n(\boldsymbol{r}_1; \boldsymbol{r}_1')\Psi_1(x') \right] \mathrm{d}r' \\ H_{\mathrm{inc}}(\boldsymbol{r}_2) &= \int_S \left[ G_n(\boldsymbol{r}_2; \boldsymbol{r}_2')\Psi_2(x') - G_n(\boldsymbol{r}_2; \boldsymbol{r}_1')\Psi_1(x') \right] \mathrm{d}r' \end{aligned} \tag{4}$$

where $G_n$ denotes the normal derivative of $G$ and

$$\begin{aligned} \boldsymbol{r}_1 &= (x, S_1(x)), \qquad & \boldsymbol{r}_1' &= (x', S_1(x')) \\ \boldsymbol{r}_2 &= (x, S_2(x)), \qquad & \boldsymbol{r}_2' &= (x', S_2(x')). \end{aligned} \tag{5}$$

The main task is to invert this set of coupled equations to find the field terms $\Psi_1$, $\Psi_2$ along the surfaces. These may then be substituted into equation (2) to yield the value of the field in the waveguide.

The incident field itself has not yet been specified. This must be obtained as an integral over the aperture:

$$H_{\mathrm{inc}}(\boldsymbol{r}_s) = \int_A G_n(\boldsymbol{r}_s, \boldsymbol{r}')p(\boldsymbol{r}') - G(\boldsymbol{r}_s, \boldsymbol{r}')p_n(\boldsymbol{r}')\,\mathrm{d}\boldsymbol{r}' \tag{6}$$

where $p$ denotes an incident plane wave, $\boldsymbol{r}_s$ is a surface point $x, S(x)$ and $n$ denotes differentiation in the direction normal to the aperture, i.e. parallel to the $x$-axis. (This represents the field which would exist beyond the aperture, in the absence of the waveguide itself.)

For convenience we now write equation (4) in operator notation,

$$\begin{aligned} H_{\text{inc}}(\boldsymbol{r}_1) &= (L_{11} + R_{11})\Psi_1 + (L_{12} + R_{12})\Psi_2 \\ H_{\text{inc}}(\boldsymbol{r}_2) &= (L_{21} + R_{21})\Psi_1 + (L_{22} + R_{22})\Psi_2 \end{aligned} \tag{7}$$

where the operators are defined by

$$\begin{aligned} L_{11} f &= \tfrac{1}{2} f(\boldsymbol{r}_1) - \int_{S_1(x' \leqslant x)} G_{\boldsymbol{n}}(\boldsymbol{r}_1; \boldsymbol{r}_1') f(\boldsymbol{r}_1')\, \mathrm{d}r', \\ R_{11} f &= - \int_{S_1(x' > x)} G_{\boldsymbol{n}}(\boldsymbol{r}_1; \boldsymbol{r}_1') f(\boldsymbol{r}_1')\, \mathrm{d}r', \\ L_{12} f &= - \int_{S_2(x' \leqslant x)} G_{\boldsymbol{n}}(\boldsymbol{r}_1; \boldsymbol{r}_2') f(\boldsymbol{r}_2')\, \mathrm{d}r', \\ R_{12} f &= - \int_{S_2(x' > x)} G_{\boldsymbol{n}}(\boldsymbol{r}_1; \boldsymbol{r}_2') f(\boldsymbol{r}_2')\, \mathrm{d}r' \end{aligned} \tag{8}$$

with the obvious definitions for $L_{21}$, $L_{22}$, $R_{21}$, $R_{22}$ from the second of equations (4). In all of these expressions the left-hand integrals $L_{ii}$ are interpreted as the Cauchy principal value.

Equations (7) can be expressed more concisely if we define the vectors $\boldsymbol{u}$ and $\boldsymbol{f}$ as the pairs of functions

$$\begin{aligned} \boldsymbol{u} &= (\Psi_1, \Psi_2), \\ \boldsymbol{f} &= (H_{\text{inc}}(\boldsymbol{r}_1), H_{\text{inc}}(\boldsymbol{r}_2)). \end{aligned} \tag{9}$$

We can then write (7) in the form

$$\boldsymbol{f} = \boldsymbol{A}\boldsymbol{u} \equiv (\boldsymbol{L} + \boldsymbol{R})\boldsymbol{u} \tag{10}$$

where $\boldsymbol{L}$ and $\boldsymbol{R}$ are the $2 \times 2$ matrix operators whose entries are integral operators $L_{ij}$, $R_{ij}$ corresponding to the above splitting, e.g.

$$\boldsymbol{L} = \begin{pmatrix} L_{11} & L_{12} \\ L_{21} & L_{22} \end{pmatrix}, \qquad \boldsymbol{R} = \begin{pmatrix} R_{11} & R_{12} \\ R_{21} & R_{22} \end{pmatrix}. \tag{11}$$

In the above expression (10) $\boldsymbol{L}$ therefore describes the scatter from the left.

The required solution of equation (10) is then given by

$$\boldsymbol{u} = (\boldsymbol{L} + \boldsymbol{R})^{-1} \boldsymbol{f}. \tag{12}$$

The main task is the inversion of $(\boldsymbol{L} + \boldsymbol{R})$. As in previous treatments [12] we make use of the assumption that the effect of $\boldsymbol{R}$ is 'small' in some sense, reflecting the fact that most of the scattering is due to interaction from the left. The solution (12) can be then expanded in a series

$$\boldsymbol{u} = [1 - \boldsymbol{L}^{-1}\boldsymbol{R} + (\boldsymbol{L}^{-1}\boldsymbol{R})^2 - \cdots]\boldsymbol{L}^{-1}\boldsymbol{f}. \tag{13}$$

Provided it converges this equation can be truncated and treated term by term. When the system is discretized, the operator $\boldsymbol{L}$ yields a lower triangular matrix operator, whose entries are simply the four lower-triangular matrices arising from $L_{ij}$. Similarly $\boldsymbol{R}$ becomes an upper triangular matrix operator (with zero on the diagonals). Inversion of the matrix $\boldsymbol{L}$ can be carried out very efficiently (using Gaussian elimination and backward substitution) to give the first term of equation (13). Since subsequent terms in the series are products of $\boldsymbol{L}^{-1}$ and $\boldsymbol{R}$, they can also be evaluated efficiently.

For predominantly right-going waves, the functions on which $\boldsymbol{R}$ operates in the series (13) will all have phases which vary rapidly with $x$, so that the right half-integral represented by $\boldsymbol{R}$ will give rise to functions whose amplitude is small, as required. It is nevertheless difficult to put rigorous bounds on surface geometry which would guarantee convergence.

## 3. Numerical solution

The numerical treatment of the equations will now be outlined briefly. The details are analogous to those given in [12] for rough surfaces.

*Discretization.* The main step is the discretization of the integral equation, and numerical solution of the resulting system. The system is first discretized with respect to $x$, choosing $N$ equally spaced points $x = x_1, \ldots, x_N$, where $x_n = n\delta$, say, and the length $\delta$ of each subinterval is small. In practice a value of 10 points per wavelength was found sufficient for $\delta$. Each integral can then be written as a sum of subintegrals over the subintervals $[x_n, x_{n+1}]$, so that for example

$$L_{11}H(\boldsymbol{r}_1) = \tfrac{1}{2}H(\boldsymbol{r}_1) - \sum_{n=1}^{N}\left[\int_{x_n}^{x_{n+1}} G_{\boldsymbol{n}}(\boldsymbol{r}_1, \boldsymbol{r}')H(\boldsymbol{r}')\,\mathrm{d}S\right].$$

These intervals can be chosen to be sufficiently small so that over each of them the unknown part of the integrand, $H(\boldsymbol{r}')$, can be treated as constant and taken outside the integral. The remaining part of the integrand is a known function which depends on the given surface profile. Writing this for each of the $N$ points $\boldsymbol{r}_s = (x_n, h(x_n))$, $n = 1, \ldots, N$ gives rise to a matrix equation, say

$$H_{\mathrm{inc}} = AH. \tag{14}$$

Now define the difference $r_{ij} = |(x_i, h(x_i)) - (x_j, h(x_j))|$, and the slope variable

$$\sigma_n = \sqrt{1 + h'(x_n)^2}$$

where the prime denotes the $x$-derivative, $h' = \mathrm{d}h/\mathrm{d}x$. The matrix entries as used in the results below are then given as follows:

$$\begin{aligned} A_{mn} &= \frac{\mathrm{i}\delta}{4}\sigma_n \left.\frac{\partial H_0^{(1)}}{\partial n}\right|_{kr_{mn}} \qquad \text{for} \quad m \neq n \\ A_{mm} &= -\left[\frac{1}{2} - \frac{\delta}{\sigma_m^2\pi}h''(x_m)\right]. \end{aligned} \tag{15}$$

Note that the off-diagonal entries $m \neq n$ have simply been approximated by the Green function, with a factor accounting for arc-length. This arises by treating the integrand as constant over the corresponding interval and is introduced to simplify the computation. It is straightforward to improve the accuracy of this, but the approximation (15) was found to be sufficient to give extremely close agreement.

*Left–right splitting.* The system (14) can now be solved using one or more terms of the series solution (13). The solution is obtained, first, for the purely right-going part, say

$$\boldsymbol{u}_1 = \boldsymbol{L}^{-1}\boldsymbol{f} \tag{16}$$

and a correction $\boldsymbol{u}_2$ to this is then calculated, by applying the integral operator $\boldsymbol{R}$ and inverting $\boldsymbol{L}$ again,

$$\boldsymbol{u}_2 = \boldsymbol{L}^{-1}(\boldsymbol{R}\boldsymbol{u}_1) \tag{17}$$

to give the solution

$$\boldsymbol{u} \cong \boldsymbol{u}_1 - \boldsymbol{u}_2.$$

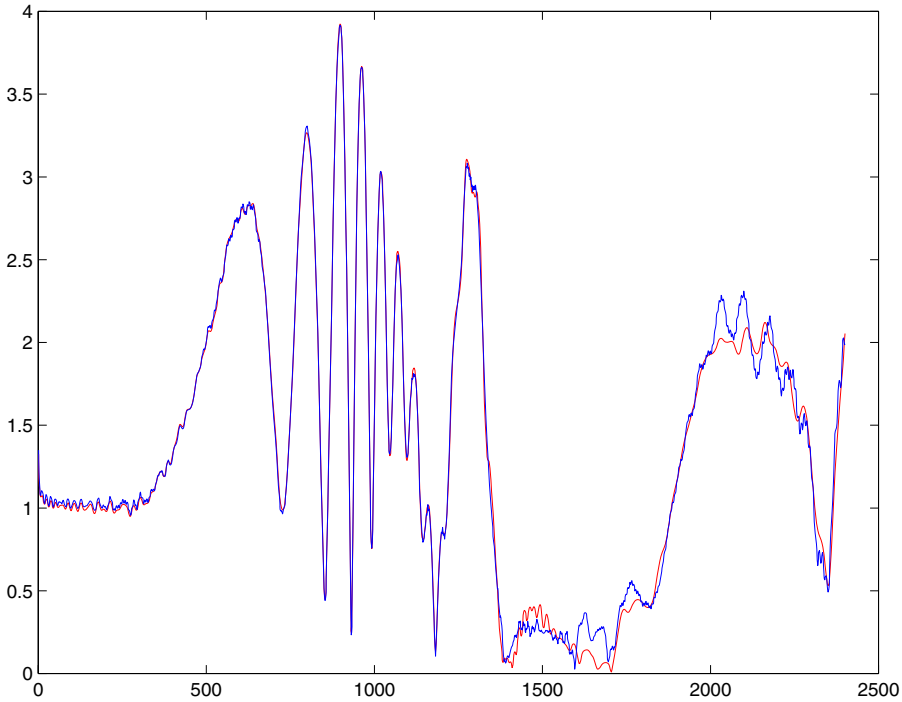


**Figure 2.** Surface currents along the upper surface, from the first two iterations.

This gives the required surface currents along the two surfaces. This is then used as the 'driving field' for the calculation of interior fields, using equation (2).

Note that for this geometry $x$ could be replaced by a coordinate $s$, say, following the curved waveguide axis. In several respects this is a more natural coordinate, particularly for waveguides which curve at greater than 90° to the $x$-axis, although for simplicity we have not done so here. (Use of the curved axis $s$ raises problems of surface grid definition when the curvature becomes large, and in fact it is possible to retain the use of the $x$-coordinate even for toroidal waveguides.)

## 4. Results

The aims of this work are to evaluate the scattering inside a long irregular waveguide, and to examine the accuracy and convergence of the series approximation, over a wide range of incident angles.

The geometry of the waveguide used in the following examples is as shown in figure 1. This consists of straight sections adjoining two sinusoidally curved sections, as illustrated. The waveguide depth at the aperture was chosen to be $20\lambda$, and the overall length (with respect to the $x$-axis) was $200\lambda$. Incident angles are measured, anticlockwise, with respect to the horizontal.

### *4.1. Surface currents and interior fields*

Current amplitude along the upper surface is shown in figure 2 for a field incident at a grazing angle of 0°, i.e. in the $x$-direction. Figure 2 shows the result of the first and second iterations.

**Figure 3.** Amplitude of the incident field using Kirchhof integral over aperture, i.e. the aperture field, inside a waveguide of diameter $20\lambda'$ over a length of $200\lambda$, for the field incident at $-20^\circ$.

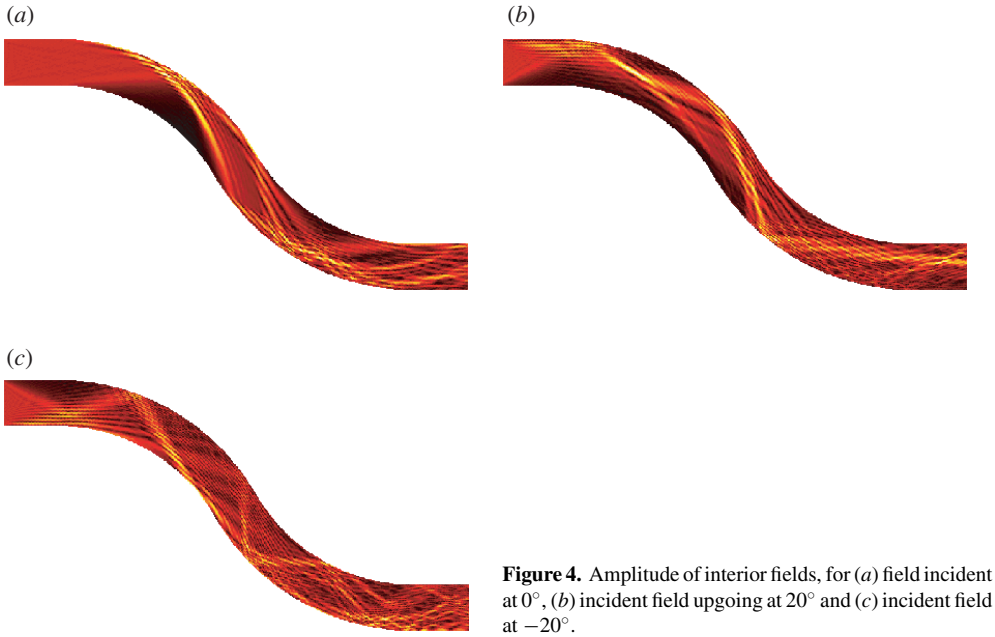


**Figure 4.** Amplitude of interior fields, for (*a*) field incident at $0^\circ$, (*b*) incident field upgoing at $20^\circ$ and (*c*) incident field at $-20^\circ$.

It is seen that these are in close agreement, except near the far end, where backscatter due to the truncation of the waveguide becomes more significant. Surface currents for non-zero angles of incidence are similar.

The aperture field itself is shown in figure 3, where edge effects due to the finite aperture are clear from the amplitude spread. (As expected, as the aperture width increases in relation to wavelength the shadow boundary becomes sharper.)

The interior field is calculated as an integral of the wall currents over the whole surface, as in equation (2).

The field amplitudes in the following graphs clearly show the extent of diffraction and multiple scattering. The amplitudes for incident angles of $0^\circ$, $20^\circ$ (upgoing) and $-20^\circ$ (downgoing) are given in figures 4(*a*)–(*c*) respectively, for which 'whispering gallery modes' are evident.

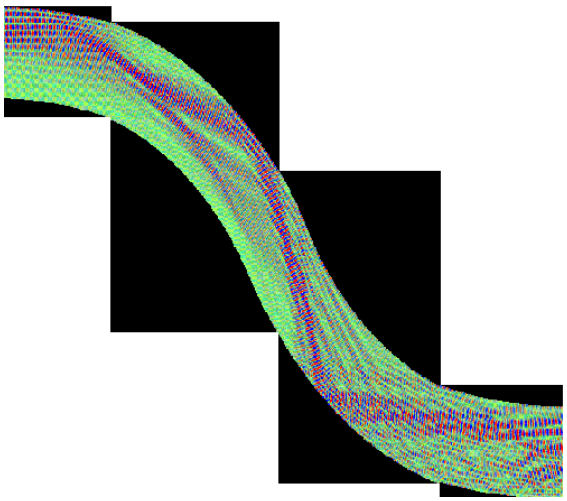

**Figure 5.** Real part of the field from BAE finite-element calculations, due to an incident wave at 20° to the horizontal.

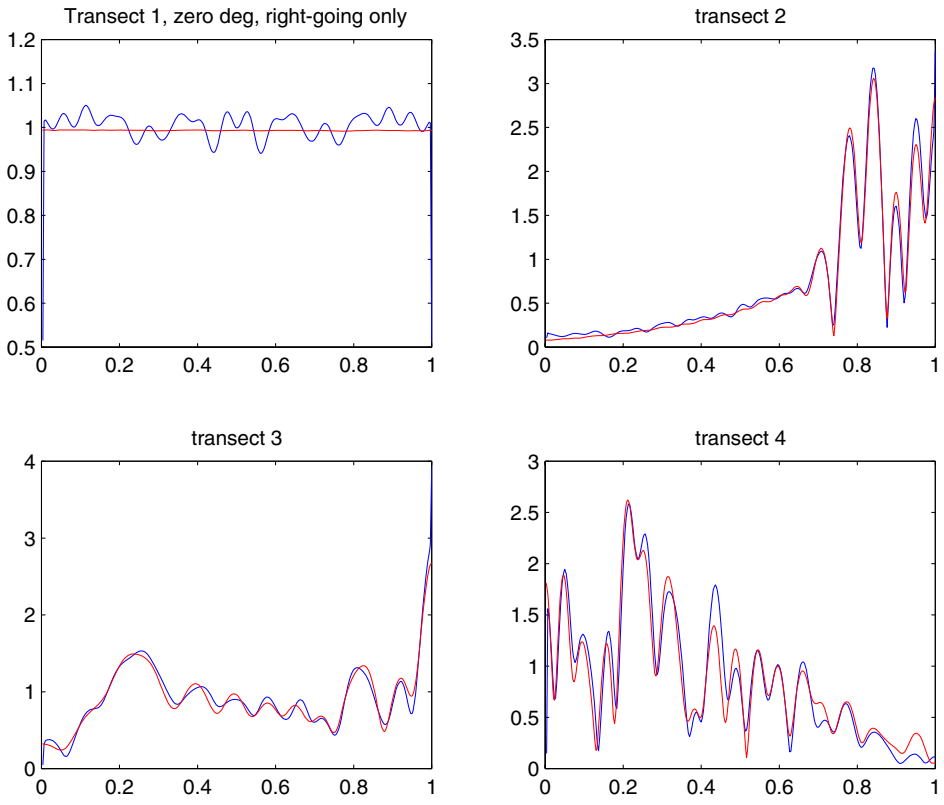


**Figure 6.** Field amplitudes compared on the first four transects for zero angle of incidence, using the first term only. The horizontal axis is scaled to unity.

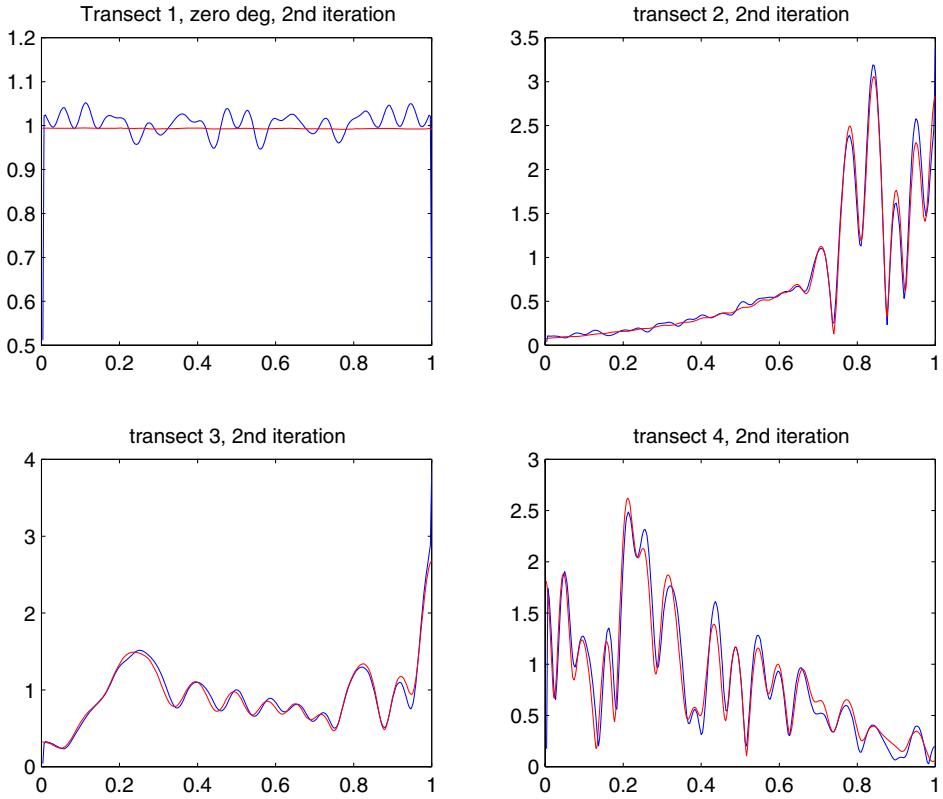


**Figure 7.** Field amplitudes compared on the first four transects for zero angle of incidence, including the second iteration.

### *4.2. Validation*

A numerical code, developed at BAE Systems, Advanced Technology Centres—Sowerby, was used to obtain a full-field solution for the waveguide. The code, LOC2D, implements a finite-volume scheme on an arbitrary unstructured grid. LOC2D allows for the use of a body conforming grid, removing the need for the 'staircasing' of the waveguide walls as in conventional finite-difference time domain (FDTD) methods, yet has an operation count close to that of FDTD schemes. The accuracy of the LOC2D method is therefore expected to be better than for FDTD as errors arising from 'staircasing' are removed. The calculation times will be comparable to those of FDTD methods. The waveguide problem was discretized at $\lambda/25$, using quadrilateral cells. The mesh was generated in six sections along the length of the waveguide and joined together to form the overall calculational mesh of around 3.2 million cells. Calculations were carried out for an TM incident plane wave (corresponding to vertically polarized electric field) at angles of incidence of $20^\circ$, $0^\circ$, $-20^\circ$ with respect to the horizontal.

Typical calculation times for the surface current calculations here were approximately 17 s for the first term in the left–right series, and around 160 s to produce the interior field plots (this figure being directly proportional to the number of field points). By comparison the calculation took several hours for the LOC2D computations on a vector machine.

Figure 5 shows the real part of the field throughout part of the waveguide for an incident angle of $20^\circ$ upgoing and can be compared with amplitude in figure 4(*b*). In order to obtain

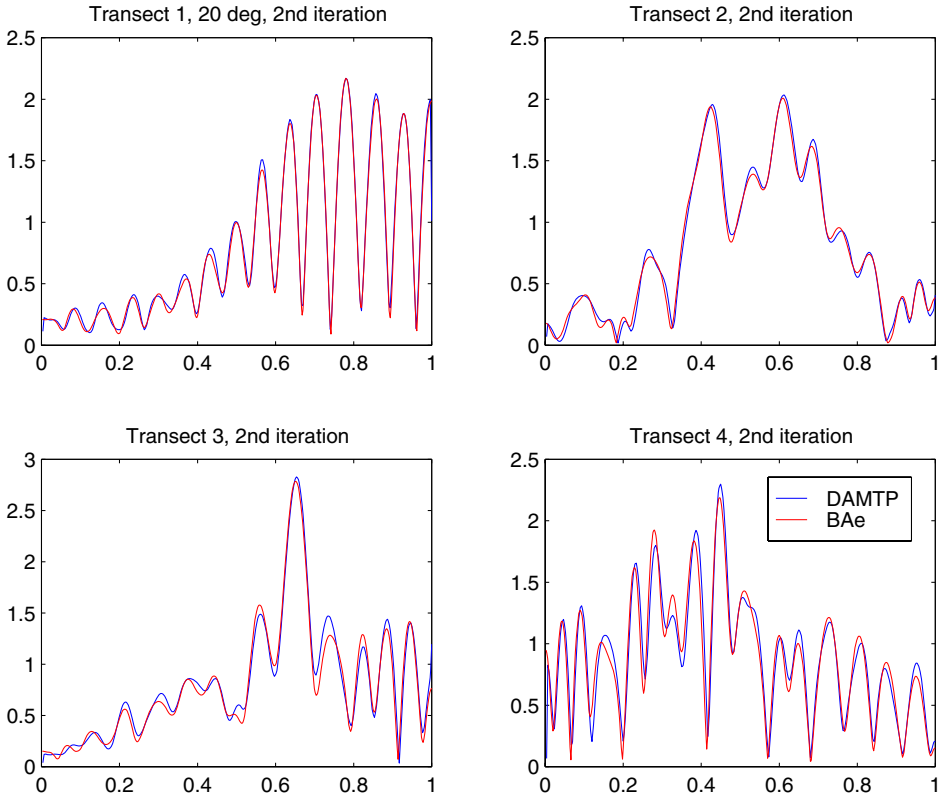


**Figure 8.** Comparison of field amplitude as in figure 7, for an upward-going incident field at an angle of 20°.

detailed quantitative comparison, full fields were evaluated on a series of five one-dimensional 'transects', crossing the waveguide at various distances. This was repeated for several angles of incidence, and representative examples are given in figures 6–9. The calculations presented here have been evaluated to include both first and second iterations. It is seen here that agreement at the second iteration is excellent in almost all cases, and in most cases the first term alone is accurate to well within 5%. Figure 6 compares the fields on the first four transects for zero angle of incidence, using the first term only. In figure 7 the same case is examined, giving the comparison when the second iteration is included. (The horizontal axis for all transect plots has been scaled to unity. In each case the field is shown along the whole transect, from one surface to the opposite surface.) The graphs provide the most compelling evidence of the accuracy of the approach. In these plots, the only apparent discrepancy is at the first transect. (This is exaggerated by the scale, and is in fact only on the order of a few per cent. It appears to be due simply to differences in representation of the incident field.) Figures 8 and 9 show the corresponding comparison, at the second iteration, for upward- and downward-going incident fields at 20° to the horizontal. The comparisons at the fifth transect near the far end of the waveguide, for each of the three angles, are shown separately in figures 10(*a*)–(*c*).

The left–right splitting method has also been compared with predictions of the interior fields from a modal method, for a three-dimensional cylinder of circular cross-section, obtaining the unknown mode amplitude by field matching across the aperture. Agreement was

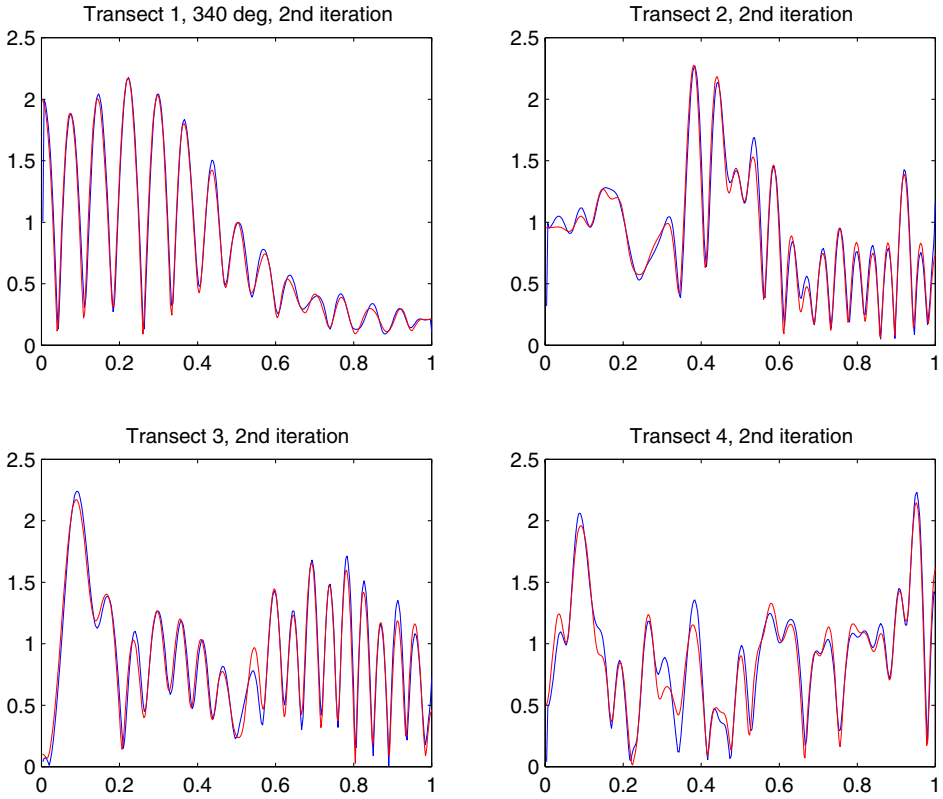


**Figure 9.** Comparison of field amplitude as in figure 7, for an incident field at an angle of $-20^\circ$.

found to be good. Results from this comparison will be the subject of a separate paper on the validation of the three-dimensional left–right splitting method.

### *4.3. Convergence at high angles of incidence*

The convergence was then examined over a wide range of angles of incidence. The method was found to converge even at $60^\circ$ from the horizontal, where reasonable convergence was reached by around the fifth or sixth iteration. The interior field pattern for this case is illustrated in figure 11.

Convergence is typically slowest near the right-hand end of the waveguide, where it is dominated by reflections. (These are largely spurious when the model is used to represent an extended waveguide.) If the solution is measured excluding this section, convergence is considerably faster.

It is most convenient to quantify convergence directly in terms of the surface currents, as the interior fields are simply obtained from these at any iteration by applying the boundary integration (2).

Denoting the surface current at the $j$th iteration by $\boldsymbol{u}_j$, convergence can be measured in several ways, all of which give similar results. One such measure is in terms of the relative successive differences $c_j = \|\boldsymbol{u}_{j+1} - \boldsymbol{u}_j\|/\|\boldsymbol{u}_j\|$, where $\|\boldsymbol{u}\|$ denotes the $L_2$-norm, i.e. the square root of sums of squares. However, the magnitude of the currents may vary enormously along the waveguide, and the quantity above may fail to detect large *percentage* differences

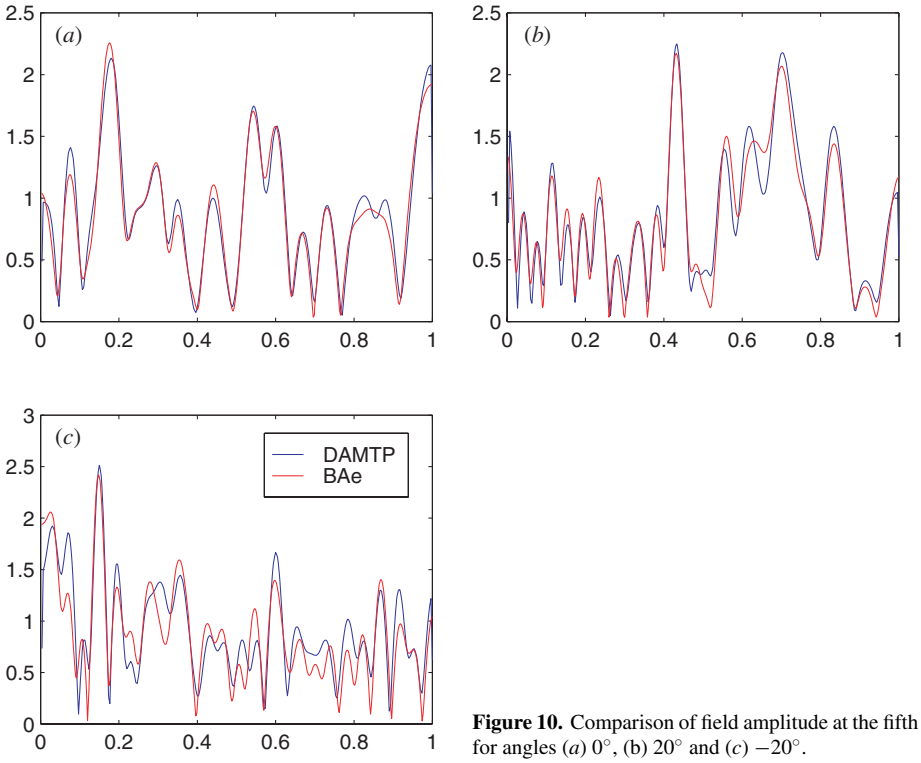


**Figure 10.** Comparison of field amplitude at the fifth transect, for angles (*a*) 0°, (b) 20° and (*c*) −20°.

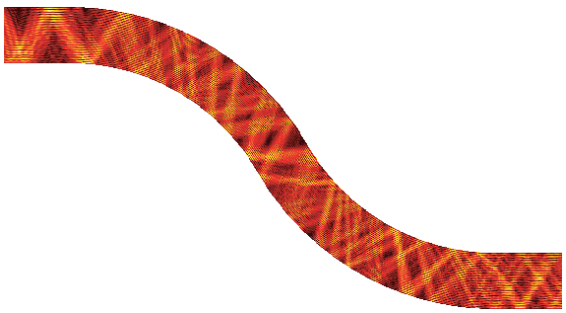

**Figure 11.** Graph of field amplitude after five iterations for a field incident at −60°.

in places where the magnitude is small. This can be remedied by normalizing pointwise, and defining $d_j = \|(\boldsymbol{u}_{j+1} - \boldsymbol{u}_j)/\boldsymbol{u}_j\|$. This quantity is shown in figure 12, for angles of incidence from 10° to 60° from the horizontal. Note that, particularly at high angles, convergence is much faster when the region around the far end is excluded from this calculation. This occurs because considerably more energy is reflected from the end at high angles. (For example at 10° angle of incidence, the first term is within around 15% of the 'exact' solution, and the solution has converged to within about 2% by the third or fourth term.)

Further insight is provided by figure 13, which shows a comparison of lower wall currents at the first, third, fifth and tenth iterations, for an incident angle of 50°. Despite the high angle, it is seen that almost all features of the wall currents are well captured even after very few iterations.

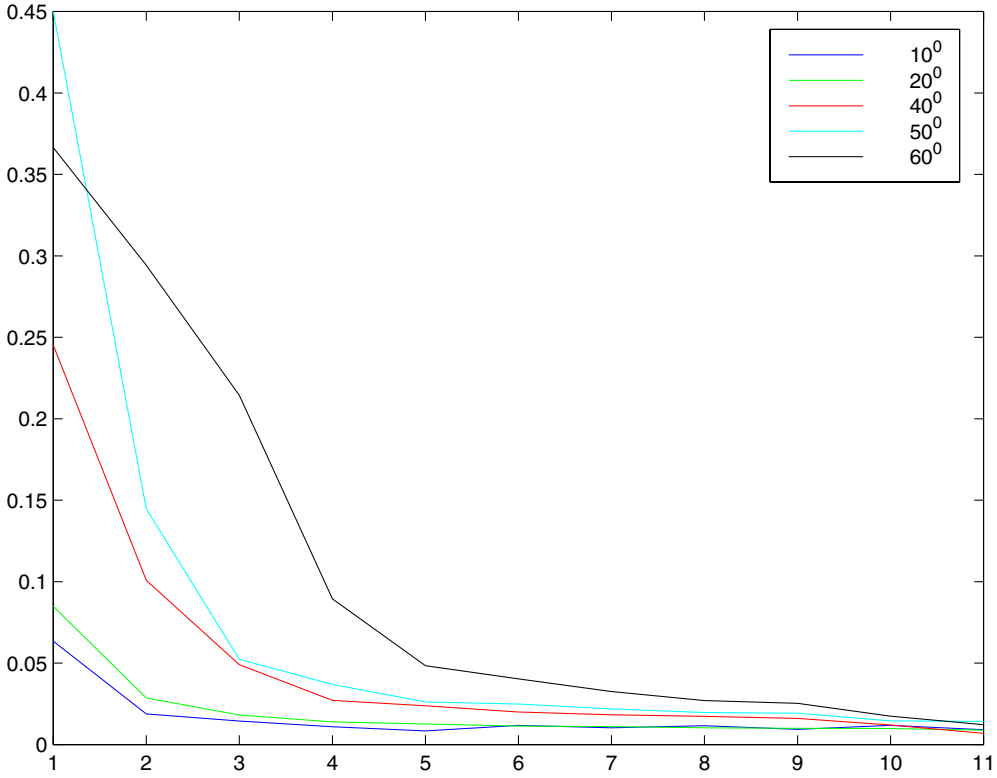


**Figure 12.** Rate of convergence shown as a function of incident angle. The horizontal axis is the iteration number, and the vertical scale is as defined in the text.

### *4.4. Rough waveguide*

A further waveguide was generated with stochastically rough walls, and the resulting fields examined. This was done in order to illustrate the flexibility of the approach, and to examine the extent to which roughness destroys the detailed diffraction pattern present in the smooth-sided case. One example of the resulting interior field is shown in figure 14, which can be compared with figure 4($c$), the equivalent calculation for a waveguide with smooth sides. In this example the rough waveguide surface has an autocorrelation length equal to the wavelength $\lambda$, and rms height of $\lambda/10$. It can be seen that although a detailed pattern remains, it is substantially changed by the irregularity of the walls, and in particular the position of highs and nulls is affected by even very slight roughness. The field amplitude along the curved central axis is shown in figure 15, where the lack of coherence is again apparent.

Note, however, that even in the absence of roughness, multiple scattering tends to have a similar effect in reducing regions of high intensity as propagation distance increases. Consequently the effect of roughness is most noticeable in the earlier part of the waveguide.

The roughness was found to have little effect on the rate of convergence with respect to the number of iterations. However, some care is needed in making such comparisons, because roughness tends to remove the sharpest peaks and nulls in the wall currents, which are dominant features in determining the rate of convergence.

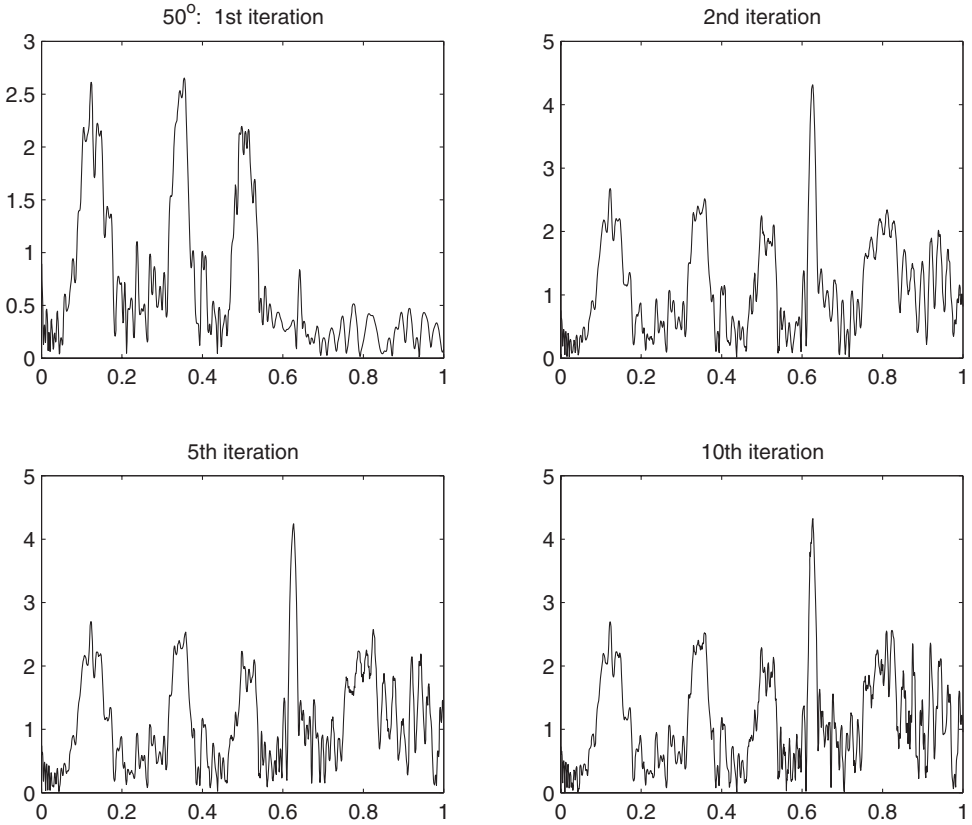


**Figure 13.** Surface current amplitudes along the length of the lower wall at several iterations, for a wave incident at 50° to the horizontal.

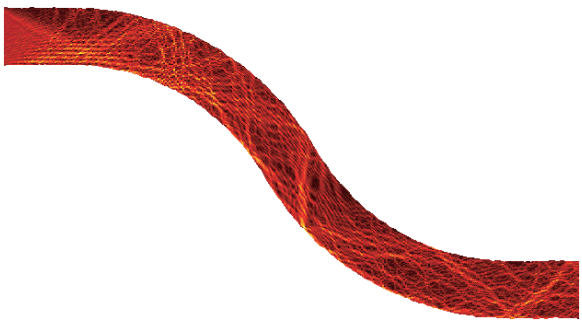

**Figure 14.** Field amplitude showing the effect of scattering in the case of a rough-sided waveguide.

## 5. Conclusions

The method of left–right splitting has been formulated and applied to a canonical problem of an irregular waveguide. This requires inversion of a pair of coupled integral equations, to yield the electric currents along the waveguide walls. The method is computationally efficient, while

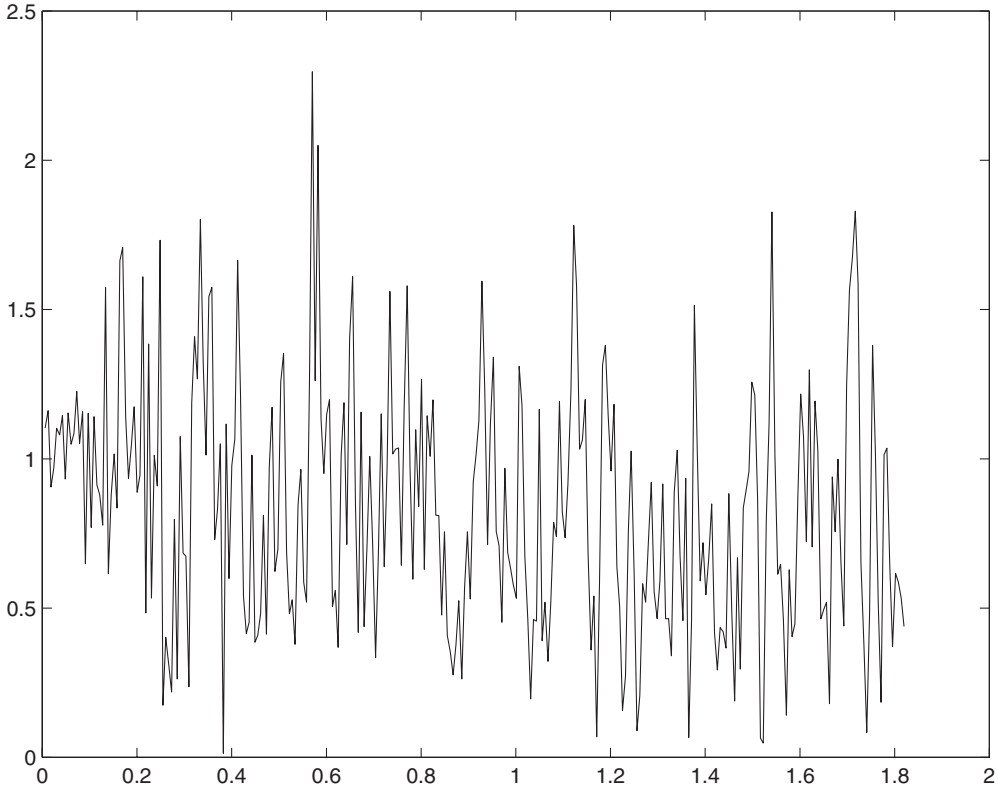


**Figure 15.** The field amplitude along the curved central axis for the example of figure 14. The horizontal axis shows the $x$-coordinate.

retaining the ability to describe high-order multiple scattering. In most cases extremely good agreement was obtained with independent calculations using one or two terms of the series. The convergence of the method was then investigated for much larger angles of incidence. It was found that even at $60^\circ$ from the horizontal the solution converges after around five iterations. Finally, the field patterns in a waveguide with rough walls were examined. As expected, diffraction effects largely destroy the detailed patterns even for slightly rough surfaces.

The method can also be applied to full three-dimensional problems, for which the computational cost and potential benefit is much greater: in the two-dimensional case, the number of discretized points $N$ scales linearly with wavenumber $k$. The main computational expense is in inversion of the governing matrix, for which the present method reduces the computational expense of 'full' inversion from $\mathrm{O}(k^3)$ to $\mathrm{O}(k^2)$. In three-dimensional problems the surface is two dimensional and the number of grid points therefore depends on the square $k^2$ of wavenumber. The computational cost of full matrix inversion (or method of moments calculations) would then be $k^6$. The present method has a computational cost of $k^3$ per matrix inversion, but this would be carried out *at each range step*, and as the range discretization also scales with $k$ this gives a further factor, so that the total cost of matrix inversions is $k^4$. This is high but still a great reduction from full inversion.

We note that the method is conceptually similar to the Bremmer series approach to inhomogeneous waveguides [13], in which the wave equation is decomposed into left- and right-going components. However, the decomposition described here applies only to surface

interactions, so that both forward and back scatter are taken into account at each iteration via the boundary integral (2).

## Acknowledgments

This work was carried out under a continuing research project on electromagnetic scattering funded by BAE SYSTEMS, Advanced Technology Centre—Sowerby. The authors are grateful to the referees for several helpful suggestions.

## References

[1] Bowman J J, Senior T B A and Uslenghi P L E 1987 *Electromagnetic and Acoustic Scattering by Simple Shapes* (New York: Hemisphere)
[2] Jones D S 1987 *Methods in Electromagnetic Wave Propagation* (Oxford: Clarendon)
[3] Berglund W and Gopinath A 2000 WKB analysis of bend losses in optical waveguides *IEEE J. Lightwave Technol.* **18** 1161
[4] Heiblum M and Harris J H 1975 Analysis of curved waveguides by conformal transformation *IEEE J. Quantum Electron.* **11** 75–83
[5] Yamamoto T and Koshiba M 1993 Numerical analysis of curvature loss in optical waveguides by finite-element method *J. Lightwave Technol.* **11** 1579–83
[6] Uscinski B J 1995 High frequency propagation in shallow water—the rough waveguide problem *J. Acoust. Soc. Am.* **98** 2702–7
[7] Spivack M 1997 Sound propagation in an irregular two-dimensional wave-guide *J. Acoust. Soc. Am.* **101** 1250–5
[8] Lord Rayleigh 1897 On the incidence of aerial and electric waves upon small obstacles and on the passage of electric waves through a circular aperture in a conducting screen *Phil. Mag.* **44** 28–52
[9] Van Bladel J 1963 Low frequency scattering by cylindrical bodies *Appl. Sci. Res.* B **10** 195–202
[10] Kapp D A and Brown G S 1996 A new numerical method for rough surface scattering calculations *IEEE Trans. Antennas Propag.* **44** 711–21
[11] Spivack M 1994 Forward and inverse scattering from rough surfaces at low grazing incidence *J. Acoust. Soc. Am.* **95** Pt 2 3019
[12] Spivack M, Keen A, Ogilvy J A and Sillence C 2001 Validation of left–right method for scattering by a rough surface *J. Mod. Opt.* **48** 1021–33
[13] de Hoop M 1995 Generalization of the Bremmer coupling series *J. Math. Phys.* **37** 3246–82